

Vortical turbulence structure and transport mechanism in a homogeneous shear flow

O. Iida, M. Iwatsuki, and Y. Nagano

Department of Mechanical Engineering, Nagoya Institute of Technology, Gokiso-cho, Showa-ku, Nagoya 466-8555, Japan

(Received 5 March 1999; accepted 31 July 2000)

Direct numerical simulations (DNS) are carried out to investigate the kinematics of vortical structures in a homogeneous shear flow, and their association with the momentum transfer is studied in detail. Longitudinal streamwise vortices are generated and conditionally averaged over all the computational region. The effects of the nonlinear term on their kinematics are investigated by comparing the DNS and Rapid Distortion Theory (i.e., RDT). As a result, some important similarities are found in the vortical structure between the homogeneous shear flow and near-wall turbulence. It is also found that the strain rate in the vortical structure, which is markedly affected by the nonlinear term, determines the transfer functions associated with the energy cascade of the turbulence. © 2000 American Institute of Physics. [S1070-6631(00)51111-8]

I. INTRODUCTION

A turbulent shear flow is one of the more common engineering flow problems investigated. In particular, the inner region of the wall turbulence, which has a large shear rate, has been the subject of many studies. Many experimental and numerical studies on wall-bounded turbulent shear flows have confirmed the existence of quasicohherent streamwise vortices.^{1,2} They are elongated in the streamwise direction and found to play an important role in generating the Reynolds stresses and their redistribution.^{2,3} Thus, a detailed study of the streamwise vortices can provide useful insights into how to construct a structure-based turbulence model as well as a rational control strategy for turbulence.

The effects of a mean velocity gradient S are represented by the ratio of the turbulence time scale l/q to the mean-shear timescale $1/S$:

$$S^* = \frac{Sl}{q}. \quad (1)$$

This dimensionless parameter is referred to as the shear-rate parameter.⁴ Here, l is a length scale for the “energy-containing” eddies, and $q = \sqrt{u_i u_i}$ is a turbulent velocity scale. When the dissipation scale q^3/ϵ ($\epsilon = \nu u_{i,j} u_{i,j}$) is used as the length scale, S^* is represented as

$$S^* = S \frac{q^2}{\epsilon}. \quad (2)$$

Lee *et al.*⁴ found that S^* gives a better indication of differences in turbulence structures of a homogeneous shear flow. The effects of S^* on the structure of the near-wall turbulence are also studied by setting the wall in motion in the flow direction to reduce the shear rate.⁵

A homogeneous shear flow has been used to study the effects of a mean shear on turbulence because there is no solid boundary to suppress the velocity fluctuations, and the effects of the mean shear are more marked (Shirani *et al.*;⁶

Rogers *et al.*;⁷ Lee *et al.*;⁴ Kida and Tanaka;^{8,9} Matsumoto *et al.*¹⁰). It is also possible to clarify the effects of nonlinear term by comparing the DNS with the rapid distortion theory (RDT) in the homogeneous shear flow. The RDT is a method, based on the linear analysis, for calculating rapidly changing turbulent flow under different kinds of distortion, such as large-scale velocity gradients, the effects of bounding surfaces, and body forces. A detailed review of the rapid distortion theory has been given by Savil¹¹ and Hunt and Carruthers.¹² Savil¹¹ focuses on the connection between RDT and other methods to study turbulence. Hunt and Carruthers¹² indicate the applicability of RDT to even slowly changing turbulent flows, and the contribution of RDT is discussed for an understanding of the similarities and persistent features of the local eddy structure found in different kinds of shear flows. Lee *et al.*⁴ performed the DNS of a homogeneous shear flow with the shear-rate parameter S^* almost equal to the value at $y^+ = 10$, and showed that low- and high-speed streaks are generated as in the near-wall turbulence. Hence, the high shear rate alone is sufficient to generate the structural characteristics of near-wall turbulence. The rapid distortion theory (RDT), which neglects the nonlinear term, is found to predict the streaky structure.⁴

Matsumoto *et al.*¹⁰ found that by comparing both the DNS and RDT results of a homogeneous shear flow, no marked differences were observed in the Reynolds shear stresses or their budgets.¹⁰ There are also studies indicating the limitation of the applicability of the RDT. Kida and Tanaka,⁹ for example, showed that when a mean shear is imposed on a homogeneous isotropic turbulence, the blob-like vortical structures are elongated in the streamwise direction to become longitudinal vortices. It was also found that the streamwise vortex generates a spanwise vorticity layer, which finally rolls up into the vortex tubes due to the Kelvin–Helmholtz instability. Hence, they demonstrated the effects of the nonlinear term on the longitudinal vortical structures in a homogeneous shear flow.

Shirani *et al.*⁶ observed the mechanism in spectral space by which the energy at high wave numbers is reconverted into that at low wave numbers, i.e., an inverse energy cascade. The mechanism of an inverse energy cascade in a homogeneous shear flow is still unexplained. Lundgren¹³ indicated that the energy cascade is associated with vortical structures. Hence, a detailed study on the kinematics of vortical structures will provide insights into the mechanism of the inverse energy cascade.

The main thrust of the paper is to determine the role of the most prominent structural feature in shear flow turbulence, streamwise vortices, in the dynamics of the Reynolds stresses. In particular, the effects of the nonlinear evolution of the vortices, distinct from their rapid distortion by the mean shear, is considered.

II. RESULTS AND DISCUSSION

A. Effects of nonlinear terms on kinematics of the longitudinal vortex

We perform both DNS and RDT analyses of a homogeneous shear flow at a low Reynolds number with grid points of $64 \times 64 \times 64$ in the streamwise (x_1), normal (x_2), and spanwise (x_3) directions. The instantaneous velocity field \tilde{u}_i is decomposed into the mean velocity U_i and perturbation u_i . In the following, all velocity fluctuations and length scales in this study are nondimensionalized by $\sqrt{S\nu/2}$ ($=5\pi/19$) and $\sqrt{2\nu/S}$ ($=2\pi/190$). The sides of the computational region L_1 , L_2 , and L_3 are $4\pi\sqrt{S/2\nu}$ ($=380$), $2\pi\sqrt{S/2\nu}$, and $2\pi\sqrt{S/2\nu}$ in the x_1 , x_2 , and x_3 directions, respectively. In both DNS and RDT, the same decaying isotropic turbulence is used as the initial condition in which the turbulent Reynolds number $Re_t = q^4/\epsilon\nu$ is about 66, where $q = 2.2$ and $\epsilon = 0.35$. The Kolmogorov length scale η is 1.30. The ratios of η to the resolution of the grid points become $\eta/\Delta x = 0.219$, $\eta/\Delta y = 0.437$, and $\eta/\Delta z = 0.437$, where Δx , Δy and Δz are the resolution in the streamwise, the normal and the spanwise directions, respectively. The largest scale of the flow is approximated by longitudinal integral scales. The integral length scale is defined as

$$L_{\alpha\beta,\gamma} = \frac{1}{\sqrt{u_\alpha^2}\sqrt{u_\beta^2}} \int R_{\alpha\beta}(r_\gamma) dr_\gamma, (\alpha, \beta, \gamma = 1, 2, 3), \quad (3)$$

where $R_{\alpha\beta}(r_\gamma)$ is the one-dimensional, two-point velocity correlation between u_α and u_β . When $L_{\alpha\alpha,\alpha}$ is defined as the longitudinal integral scale in the x_α direction, the ratios of $L_{\alpha\alpha,\alpha}$ to the side of the computational region become $L_{11,1}/L_1 = 0.0374$, $L_{22,2}/L_2 = 0.0745$ and $L_{33,3}/L_3 = 0.0869$, where L_1 , L_2 and L_3 are the sides of the computational region in each direction.

Direct numerical simulation is carried out with a pseudo-spectral code developed by Rogallo¹⁴ for a homogeneous turbulence. The remeshing of the grid system is used to avoid its distortion. The resulting alias error is removed by a combination of a phase shift and a truncation of high wavenumbers. RDT was computed by the same DNS code. In both cases of DNS and RDT, remesh was done at $St = 1, 3$ and 5 .

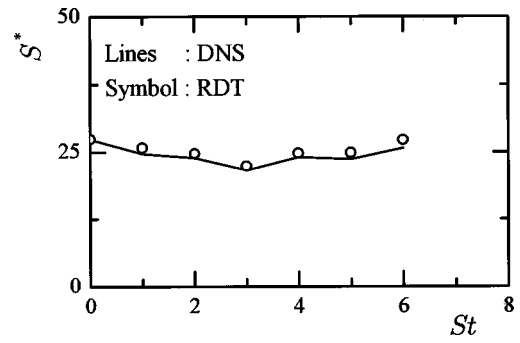


FIG. 1. Time evolution of S^* .

Time evolutions of the shear-rate parameter S^* ($=Sq^2/\epsilon$) and anisotropy of the Reynolds stresses b_{ij} are shown in Figs. 1 and 2, respectively. The anisotropy tensor of the Reynolds stresses is defined as

$$b_{ij} = \frac{\overline{u_i u_j}}{q^2} - \frac{1}{3} \delta_{ij}. \quad (4)$$

For comparison, b_{ij} of a turbulent channel flow³ is also shown in Fig. 2. In the turbulent channel flow, S^* becomes $5 \sim 30$ in the buffer region $10 \leq y^+ \leq 40$, while in the logarithmic region $y^+ > 40$, S^* is below 5 (see Lee *et al.*⁴). At the time $St = 6$ when the turbulence structure will be discussed later in detail, both S^* and b_{ij} take almost the same values at the buffer region where quasi-streamwise vortices are often observed. Moreover, no difference is observed between DNS and RDT results, indicating that the effects of nonlinear terms do not clearly appear in the second-order

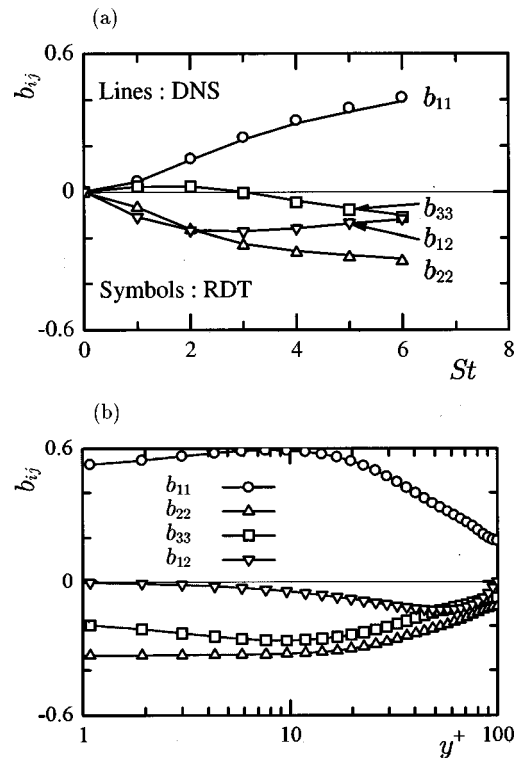


FIG. 2. Time evolution of b_{ij} . (a) Homogeneous shear flow and (b) turbulent channel flow of $Re_\tau = 100$ (Ref. 3).

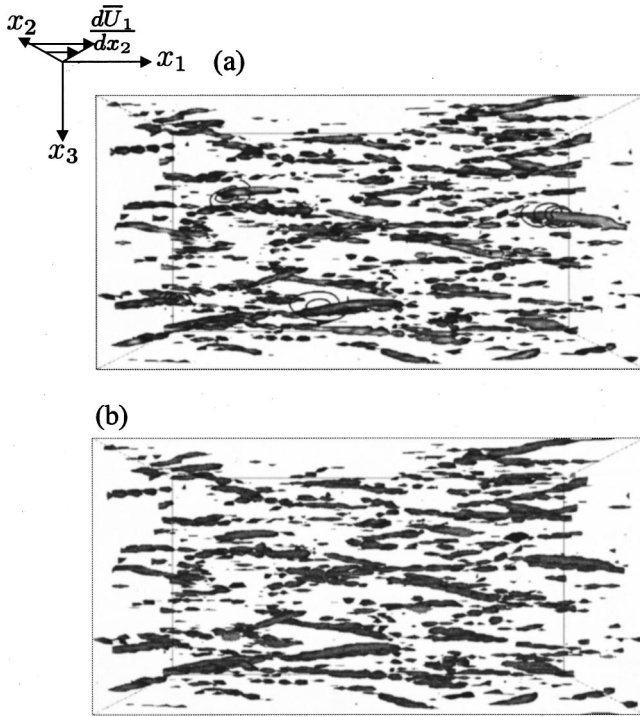


FIG. 3. The three-dimensional distributions of the vortical structures in homogeneous shear flow ($St=6$) and the streamlines around them. (a) Iso-surfaces of the second invariant of the deformation tensor $\Pi=1.0$ ($\Pi/\Pi_{rms}=3.0$), and (b) the isosurfaces of the second largest eigenvalue $\lambda_2=-0.5$.

moments of the turbulence statistics, as discussed in Matsumoto *et al.*¹⁰ At $St=6$ of DNS, $\eta/\Delta x=0.164$, $\eta/\Delta y=0.328$, and $\eta/\Delta z=0.328$, while $L_{11,1}/L_1=0.0831$, $L_{22,2}/L_2=0.116$, and $L_{33,3}/L_3=0.0238$.

Next, the vortical structures are investigated by using both the second invariant Π of the deformation tensor, which are defined as

$$\Pi = -\frac{\partial u_i}{\partial x_j} \frac{\partial u_j}{\partial x_i} = \frac{1}{2} \omega_i \omega_i - s_{ij} s_{ji}, \quad (5)$$

where $s_{ij} = 1/2(\partial u_i/\partial x_j + \partial u_j/\partial x_i)$, $\omega_i = \epsilon_{ijk} \partial u_j/\partial x_k$. As indicated by many studies, the cores of the vortices correspond well to the regions $\Pi > 0$ ^{2,8,15-17} in the wall turbulence as well as the homogeneous shear flow.

Figures 3(a) and 3(b) show the instantaneous distribution of the vortical structures in the homogeneous shear flow of DNS. The typical streamlines around the isosurfaces of Π are plotted to show that they represent the vortical structures. All streamlines are streamlines of the perturbation velocity fields alone. It is demonstrated in Fig. 3(a) that the vortical structures are elongated in the streamwise direction to become longitudinal vortices in a homogeneous shear flow. As discussed in Fig. 4, the elongation of the vortical structures is also observed without the nonlinear term, and hence is not an effect of the nonlinear terms.⁹

Recently, the vortical structures in the fully developed turbulence are also found to be detected by the isosurfaces of the second largest eigenvalue λ_2 on the tensor, $s_{ik} s_{kj} + \Omega_{ik} \Omega_{kj}$, here $s_{ij} = (u_{i,j} + u_{j,i})/2$ and $\Omega_{ij} = (u_{i,j} - u_{j,i})/2$

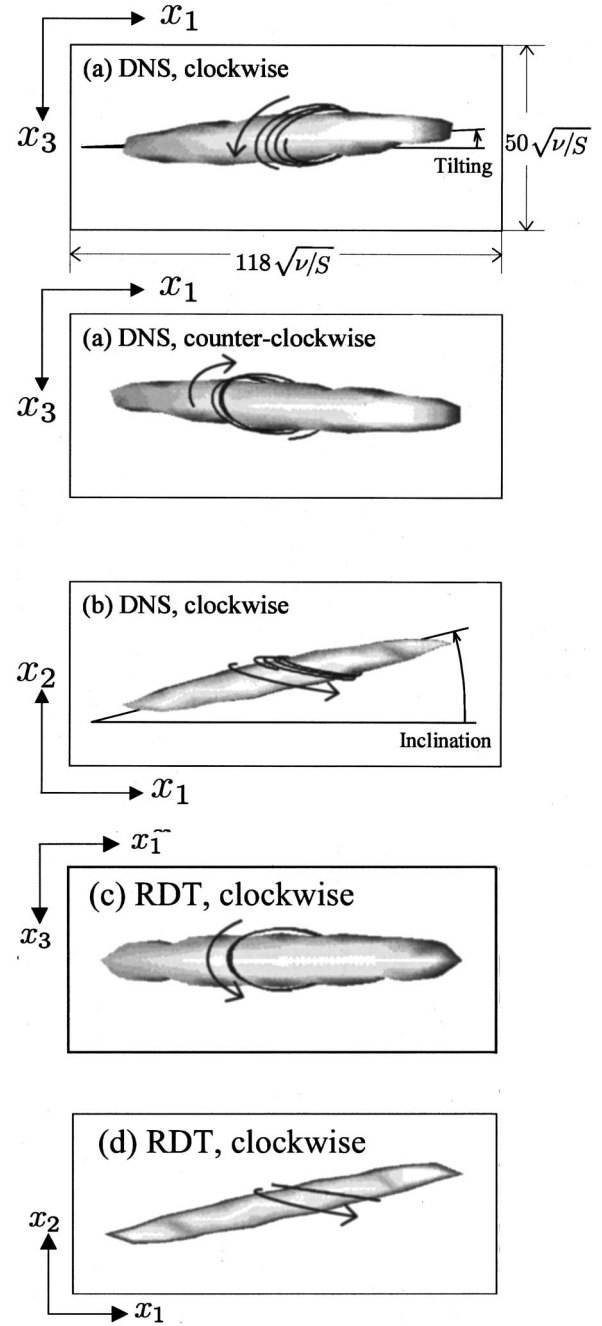


FIG. 4. The isosurfaces for $\Pi=0.16$ and the three-dimensional streamlines. (a) The top view (DNS result, $\Pi/\Pi_{rms}=0.5$), (b) side view (DNS result), (c) top view (RDT result, $\Pi/\Pi_{rms}=0.6$), and (d) side view (RDT result)

are the symmetric and the antisymmetric parts of the velocity gradient tensor $u_{i,j} = \partial u_i/\partial x_j$. Jeong *et al.*¹⁸ found that the coherent vortices are well represented by connected regions where λ_2 locally takes the negative value. Figure 3(b) shows the instantaneous distribution of negative λ_2 . However, in this case, there is no definite difference observed in comparison to the definition using Π .

Then, the numerous vortical structures are educed by using the positive Π in the homogeneous shear flow at $St=6$, and conditionally averaged over the entire flow field to yield the most likely effects of the strain-rate tensor on the longitudinal vortices. The method of conditional averaging is based on the procedures used in Jeong *et al.*¹⁸ and summa-

ized as follows: (1) Detection of the local maximum of the second invariant II in the cross-streamwise planes (positive II is used to identify the vortical structure, while the streamwise vorticity ω_1 is used to distinguish between structures with a different sense of rotation); (2) linking the local maximum of II as the core of the longitudinal vortex; (3) when the local maximum point of II in the cross-streamwise plane shifts by more than two grid points from the cross-streamwise plane of one step before, the structure is considered to be terminated and detection of a new vortical structure begins; (4) each vortex must have a streamwise length greater than $1/13L_1$, which is approximated as the integral scale $L_{11,1}$ at $St=6$ (the condition required to capture the fully developed longitudinal vortices); and (5) the educed vortical structures are averaged with the sense of rotation by aligning the midpoint of their streamwise extent.

When the DNS flow field is used, the number of vortical structures educed is $192 + 183$ (the clockwise and anticlockwise vortices). In RDT, almost the same number of clockwise and anticlockwise vortices are detected as in the DNS. Figures 4(a)–4(d) show the conditionally averaged longitudinal vortices. [Figures 4(a) and 4(b) represent the vortical structure of DNS from different viewpoints, while the RDT result is shown in Figs. 4(c) and 4(d).] The second invariant of the deformation tensor and streamlines are calculated by the conditionally averaged fluctuating velocity fields. The rms value of II , i.e., II_{rms} , in DNS and RDT are 0.314 and 0.256, respectively. The averaged vortical structure is associated with the relatively small value of II in comparison to the instantaneous vortical structures (see Figs. 3). This is because in the averaging procedure, almost all streamwise vortices are averaged even if they have the small positive value of II .

In both DNS and RDT results, the isosurfaces are elongated in the x_1 direction (the streamwise direction), and the wrapping of streamlines around them is clearly observed. Hence, the nonlinear term is not required to generate the elongated vortical structures, although a difference in the streamline does exist between DNS and RDT. The streamline of DNS becomes spiral and is stretched in the streamwise direction, indicating that the longitudinal vortex is under the effects of the strain rate $\partial u_1 / \partial x_1 > 0$, i.e., nonlinear vortex stretching.

When the inclination and tilting angles are defined as the schematics of Fig. 5, it is found that in the $x-z$ plane the longitudinal vortices with a positive (negative) ω_1 tend to tilt at a positive (negative) angle, while all of them are inclined at the positive angle in the $x-y$ plane. A similar inclination and tilting of the longitudinal vortices are observed in the turbulent channel flow.¹⁸ RDT can predict the inclination of the longitudinal vortex, while the tilting does not occur without an effect of the nonlinear terms.

The vortical structure is discussed by using the vortex lines, which contain the mean velocity. Figure 6 shows the vortex lines around the averaged vortical structures in both cases of DNS and RDT. The vortex lines traced from outside of the coherent vortices generate the hairpin-like curvatures. However, we cannot observe any definite difference between DNS and RDT. The hairpin-like curvature of the vortex lines

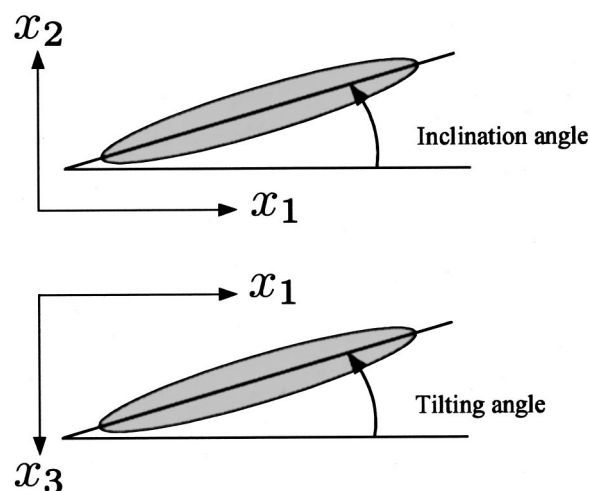


FIG. 5. Schematics for the definitions of inclination and tilting angles (Ref. 18).

was found by Rogers *et al.*⁷ in the direct numerical simulation of the homogeneous shear flow. They also discussed the similarity of the vortical structure between the boundary layer and homogeneous shear flow.

They are generated because ω_2 bends the vortex lines into the x_2 direction. However, the large value of ω_2 is as-

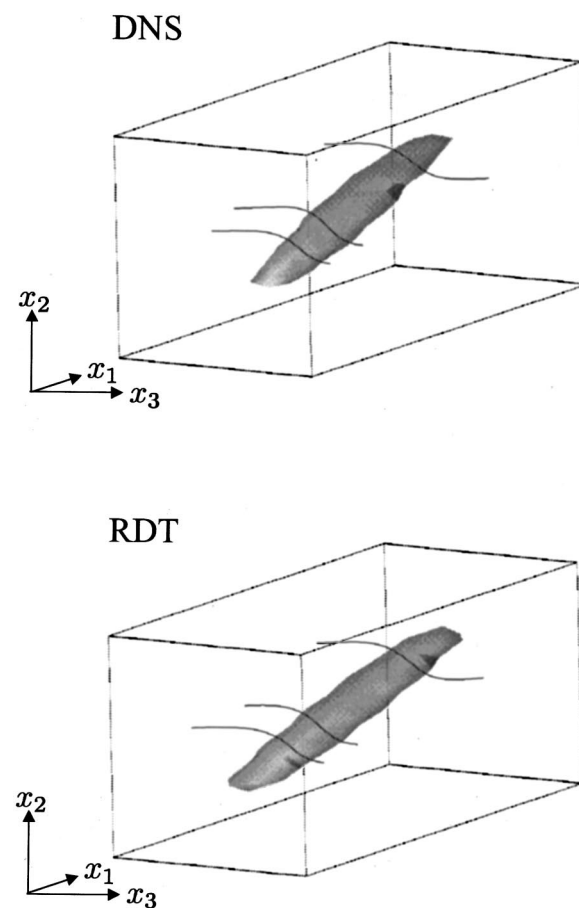


FIG. 6. The vortex lines around the conditionally averaged streamwise vortices. The isosurfaces are same as the ones used in Fig. 4.

sociated with the low- and high-speed fluids pumped up by the swirling motion of the streamwise vortices. This is obvious from the figures because there is only one streamwise vortex conditionally educed in the domain of both DNS and RDT.

B. Effects of the kinematics of the vortical structures on the redistribution term

Next, the three-dimensional kinematics of the vortical structure are investigated using both the second invariant II of the deformation tensor and the third invariant III' of the strain-rate tensor, which is defined as

$$III' = -s_{ij}s_{jk}s_{ki}. \quad (6)$$

The third invariant of the strain-rate tensor represents the detailed kinematics of the vortical structures,¹⁵ which are closely associated with the strain rate imposed on them. The sign of III' is determined by the largest eigenvalue of the strain rate tensor. When it takes a positive (negative) value, III' becomes negative (positive). A previous DNS study on the kinematics of the vortical structure showed that the largest eigenvalue tended to become negative, and that the others were positive in the vortical regions.¹⁹

Figure 7(a) shows the joint probability density function (p.d.f.) between II and III' in the isotropic turbulence used as the initial condition, while the results of a homogeneous shear flow are seen in Figs. 7(b) and 7(c). In the isotropic turbulence at a very low Reynolds number, III' becomes almost zero in the positive II regions, indicating that the vortical structures are without the strain rate and are in solid-body rotation. A homogeneous shear flow has a larger III' than an isotropic turbulence. The comparison between DNS and RDT shows that III' of DNS tends to become positive at the region of the large II , irrespective of its sign. Hence, in the vortical region $II > 0$, the largest eigenvalue of the strain-rate tensor takes a negative value, which agrees well with the previous DNS studies on both homogeneous shear and isotropic turbulence.¹⁹ The inclination of III' toward the positive value is not observed in RDT.

Because the nonlinear term seriously affects the strain-rate tensor, each component of the strain-rate tensor in the vortical region is then studied. Figure 8 shows the expected value of the strain-rate tensor versus the second invariant of the deformation tensor. In the figure, $W_X(Y)$ is defined as follows:

$$W_X(Y) \equiv \int_{-\infty}^{\infty} X P(X, Y) dX, \quad (7)$$

where the parameter P is the p.d.f. of the variables X and Y , which in Fig. 8 represent s_{ij} and II , respectively. Marked differences are observed between DNS and RDT in the distribution of all diagonal components $s_{\alpha\alpha}$, and one off-diagonal component s_{12} . In the region $II > 0$ of DNS, each component of the strain-rate tensor is expected to satisfy the following relations:

$$s_{11}, s_{33} > 0, \quad s_{22}, s_{12} < 0. \quad (8)$$

In RDT, all its components become almost zero.

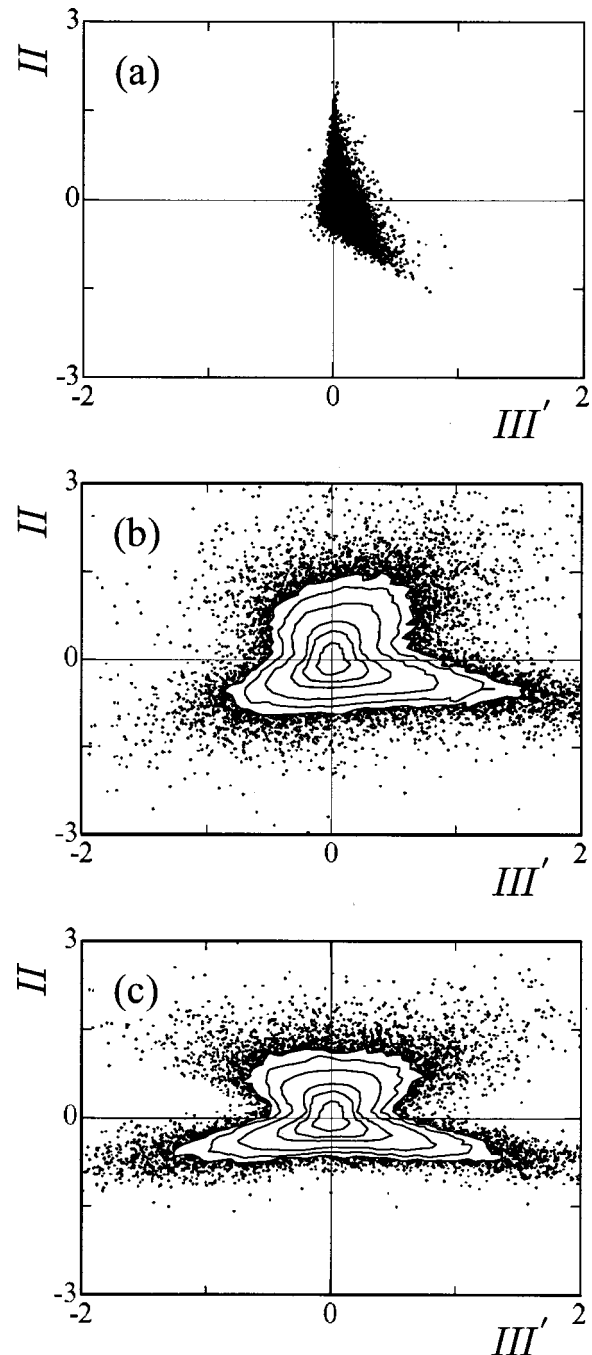
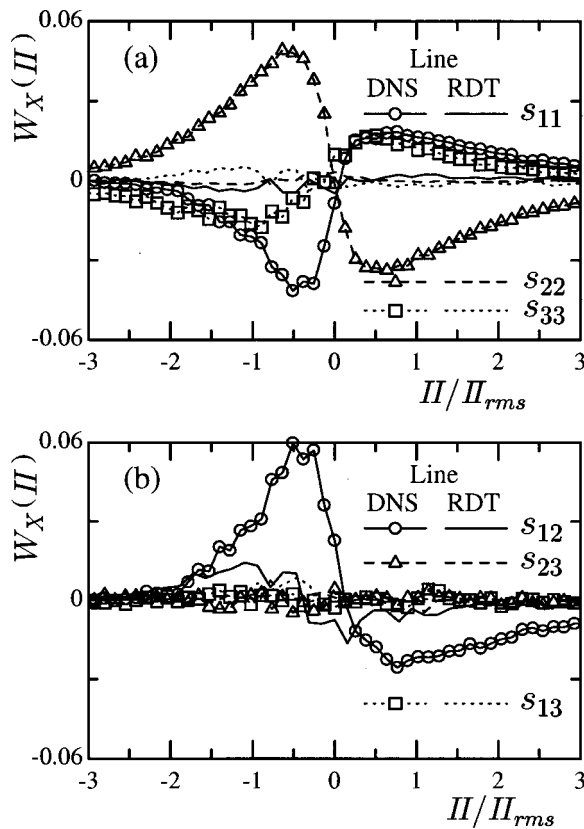


FIG. 7. Joint pdfs of II and III' . (a) $St=0.0$, (b) DNS at $St=6.0$, and (c) RDT at $St=6.0$.

We then discuss the association between the strain rate and the kinematics of the vortical structure. Figure 9 shows the distribution of the streamwise velocity fluctuation around the averaged vortices in the cross-streamwise plane, which demonstrates how $s_{12} \sim 1/2 \partial u_1 / \partial x_2$ becomes negative in the vortical structures. Typical streamlines are superimposed to show that the swirling motions are educed by the second invariant of the deformation tensor. It is noted that in both DNS and RDT results, the low- and high-speed fluids are associated with the upward and downward motions of the coherent vortices, respectively. Thus, the streamwise velocity fluctuations are found to be generated by the vertical mo-

FIG. 8. The expected value of s_{ij} vs II .

tion, which goes across the imposed mean flow. With the nonlinear convective term, the resulting velocity fluctuations are further transported by the swirling motion of the vortices. This process makes $\partial u_1/\partial x_2$ largely negative in the vortex, a phenomenon called wrapping.^{20,21} The generation mechanism of negative $\partial u_1/\partial x_2$ inside the streamwise vortices is also discussed in Kida and Tanaka⁹ by using the vorticity equation on ω_3 , because $\omega_3 = \partial u_2/\partial x_1 - \partial u_1/\partial x_2$ is almost equal to $-\partial u_1/\partial x_2$, even in the instantaneous flow field of a homogeneous shear flow.

Figures 10(a)–10(d) show the instantaneous distribution of the strain-rate tensor, $\partial u_1/\partial x_1$, $\partial u_2/\partial x_2$, and $\partial u_3/\partial x_3$, respectively. It is found that in the core of the streamwise vortex, $\partial u_1/\partial x_1 > 0$, $\partial u_2/\partial x_2 < 0$, and $\partial u_3/\partial x_3 > 0$, which is in accordance with the results of Fig. 8. The positive value of

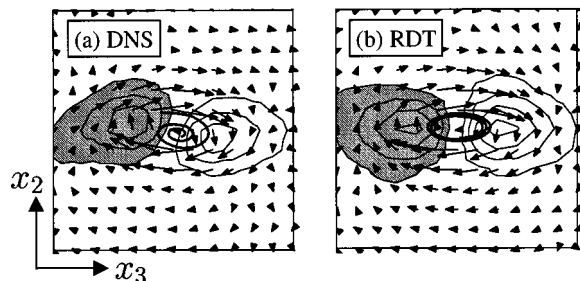


FIG. 9. Velocity vectors, typical streamlines, and contours of u_1 in the x_2 - x_3 plane. The contour lines are plotted (a) from -3.0 to 3.0 with an increment of 1.0 , and (b) from -4.0 to 4.0 with an increment of 1.0 . The shaded regions represent the negative value of u_1 .

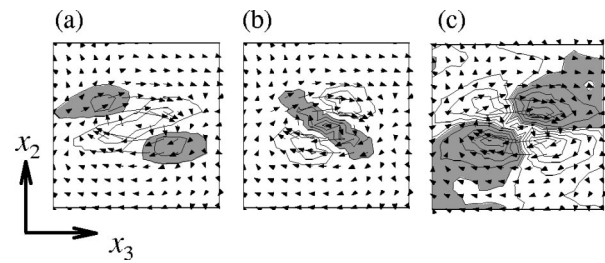


FIG. 10. Velocity vectors and contours of the strain-rate tensor in the same x_2 - x_3 plane as Fig. 9. (a) Contours of $\partial u_1/\partial x_1$ from -0.15 to 0.15 with an increment of 0.05 , (b) contours of $\partial u_2/\partial x_2$ from -0.15 to 0.1 with an increment of 0.05 , and (c) contours of $\partial u_3/\partial x_3$ from -0.16 to 0.16 with an increment of 0.05 . All figures are the results of DNS. The shaded regions represent the negative value.

$\partial u_1/\partial x_1$ results in the vortex stretching, which is clearly observed by the spiral streamlines around the averaged vortical structure of DNS (see Fig. 9). When the pure strains $\partial u_2/\partial x_2 < 0$, $\partial u_3/\partial x_3 > 0$ are imposed on the vortex, its streamline becomes elliptic and the Reynolds shear stress $-u_2u_3$ distributions show spatial variations in the vortex. Figures 11(a)–11(d) show the instantaneous $-u_2u_3$ distribution in the same cross-streamwise plane as in Fig. 9. The result of RDT shows that the contours of $-u_2u_3$ assume a cloverleaf pattern with an alternative sign, so that the spatial averaged Reynolds stress, $-u_2u_3$, must vanish. In contrast, the DNS result shows that $-u_2u_3$ is predominantly positive and negative for the clockwise and anticlockwise vortices, respectively, which is associated with the strain rates $\partial u_2/\partial x_2 < 0$ and $\partial u_3/\partial x_3 > 0$ inside the vortex.

The above discussed strain-rate tensor in the vortical structures contributes to the slow pressure-strain terms

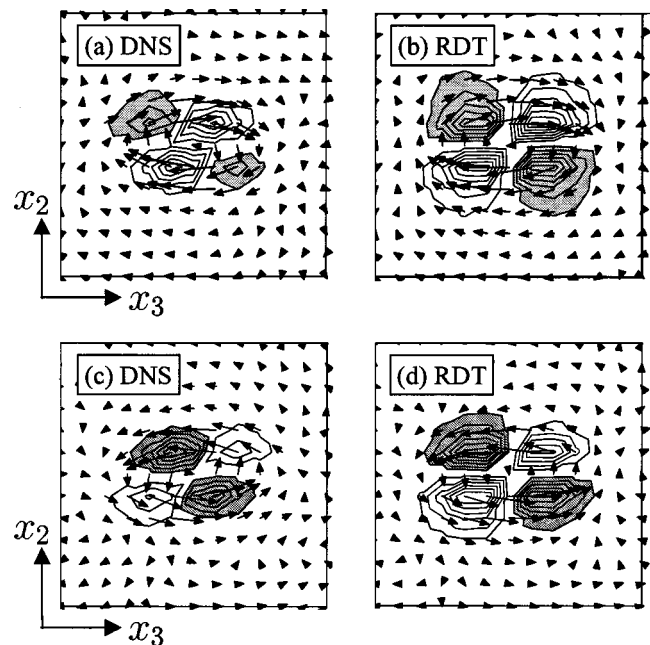


FIG. 11. Velocity vectors and contours of $-u_2u_3$ in the x_2 - x_3 plane. The contour lines are plotted (a) from -0.75 to 1.25 with an increment of 0.25 , (b), (d) from -0.6 to 0.6 with an increment of 0.1 , and (c) from -1.25 to 0.75 with an increment of 0.25 . The shaded regions represent the negative value of $-u_2u_3$.

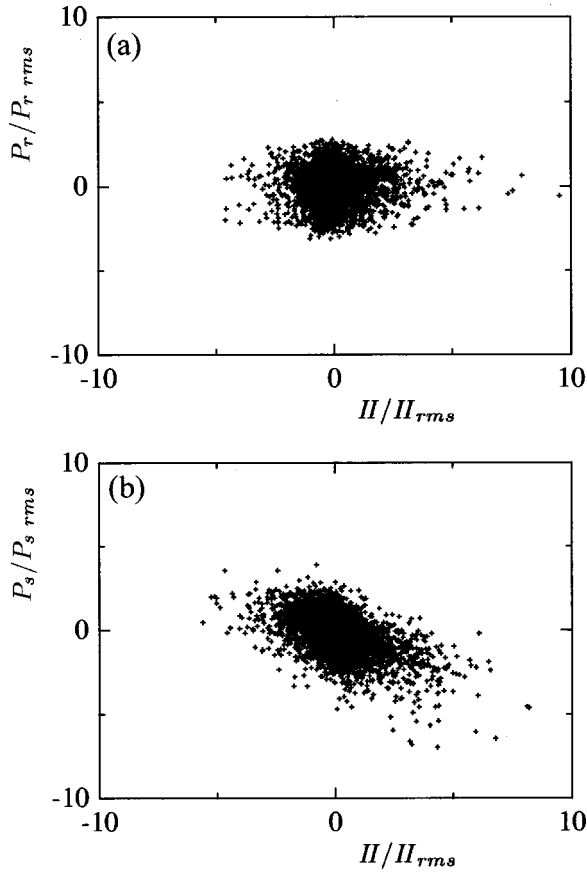


FIG. 12. The joint pdfs between the pressures and the second invariant of the deformation tensor.

$2(p_s/\rho)\partial u_\alpha/\partial x_\alpha$ included in the transport equation of the Reynolds stresses. The slow pressure–strain correlation is known to contribute to the redistribution of the Reynolds stresses and make the turbulence isotropic. The pressure p in homogeneous shear turbulence can be divided into the slow and rapid terms solved by the following Poisson equations:

$$\nabla^2 \frac{p_s}{\rho} = -\frac{\partial u_i}{\partial x_j} \frac{\partial u_j}{\partial x_i}, \quad \nabla^2 \frac{p_r}{\rho} = -2S \frac{\partial u_2}{\partial x_1}. \quad (9)$$

Figures 12(a) and 12(b) show the joint pdfs of DNS between each pressure and the second invariant of the deformation tensor. The correlation between p_s and Π is found to be very close. In the region of $\Pi > 0$, p_s tends to become negative, indicating that the slow pressure is well correlated with the vortical structure. On the other hand, the association is negligible between p_r and Π . Figure 13 shows the expected value of $2(p_s/\rho)\partial u_\alpha/\partial x_\alpha$ vs Π . Assuming the vortex cores to be associated with slow low-pressure regions, the diagonal components of the pressure–strain correlation become

$$2(p_s/\rho)\partial u_1/\partial x_1 < 0, \quad 2(p_s/\rho)\partial u_2/\partial x_2 > 0, \\ 2(p_s/\rho)\partial u_3/\partial x_3 < 0. \quad (10)$$

The distributions of the pressure–strain correlation given by Eq. (10) are again interestingly similar to those observed in the quasistreamwise vortices in the near-wall region (Figs. 17, 18, and 19 in Kasagi *et al.*¹⁷ and Fig. 19 in Jeong *et al.*¹⁸).

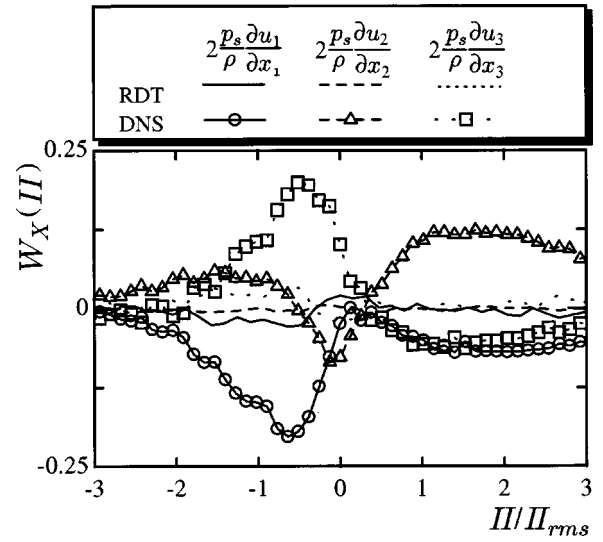


FIG. 13. Distribution of the expected value of $2(p_s/\rho)\partial u_\alpha/\partial x_\alpha$ vs Π .

C. Effects of the kinematics of the vortical structure on energy transfer function

The energy transfer functions defined in Eq. (11) are third-order moments, and hence the effects of the nonlinear term can be clearly observed,

$$\begin{aligned} \hat{T}_{\alpha\alpha} &= -\hat{u}_\alpha \left(u_k \frac{\partial \hat{u}_\alpha}{\partial x_k} \right)^* - \hat{u}_\alpha^* \left(u_k \frac{\partial \hat{u}_\alpha}{\partial x_k} \right), \quad (\alpha=1,2,3) \\ &= \underbrace{-\hat{u}_\alpha \left(u_1 \frac{\partial \hat{u}_\alpha}{\partial x_1} \right)^* - \hat{u}_\alpha^* \left(u_1 \frac{\partial \hat{u}_\alpha}{\partial x_1} \right)}_{\hat{T}_{\alpha\alpha,1}} \\ &\quad - \underbrace{\hat{u}_\alpha \left(u_2 \frac{\partial \hat{u}_\alpha}{\partial x_2} \right)^* - \hat{u}_\alpha^* \left(u_2 \frac{\partial \hat{u}_\alpha}{\partial x_2} \right)}_{\hat{T}_{\alpha\alpha,2}} \\ &\quad - \underbrace{\hat{u}_\alpha \left(u_3 \frac{\partial \hat{u}_\alpha}{\partial x_3} \right)^* - \hat{u}_\alpha^* \left(u_3 \frac{\partial \hat{u}_\alpha}{\partial x_3} \right)}_{\hat{T}_{\alpha\alpha,3}} \end{aligned} \quad (11)$$

Equation (11) gives the (inviscid) time derivative of the spectra of terms that contribute to the velocity component variances (the diagonal elements of the Reynolds stress tensor). From these spectra, we determine which terms dominate the evolution of the Reynolds stresses, and whether they move energy up or down the scale.

Figures 14(a), 14(b), and 14(c) show the distributions of the spectral energy transfer functions \hat{T}_{11} , \hat{T}_{22} , and \hat{T}_{33} , respectively. Hereafter, all wave numbers are nondimensionalized by S and ν . By comparing DNS and RDT results in \hat{T}_{11} and \hat{T}_{33} , it is found that, with the nonlinear term (DNS), the energy cascade from low to high wave numbers is mark-

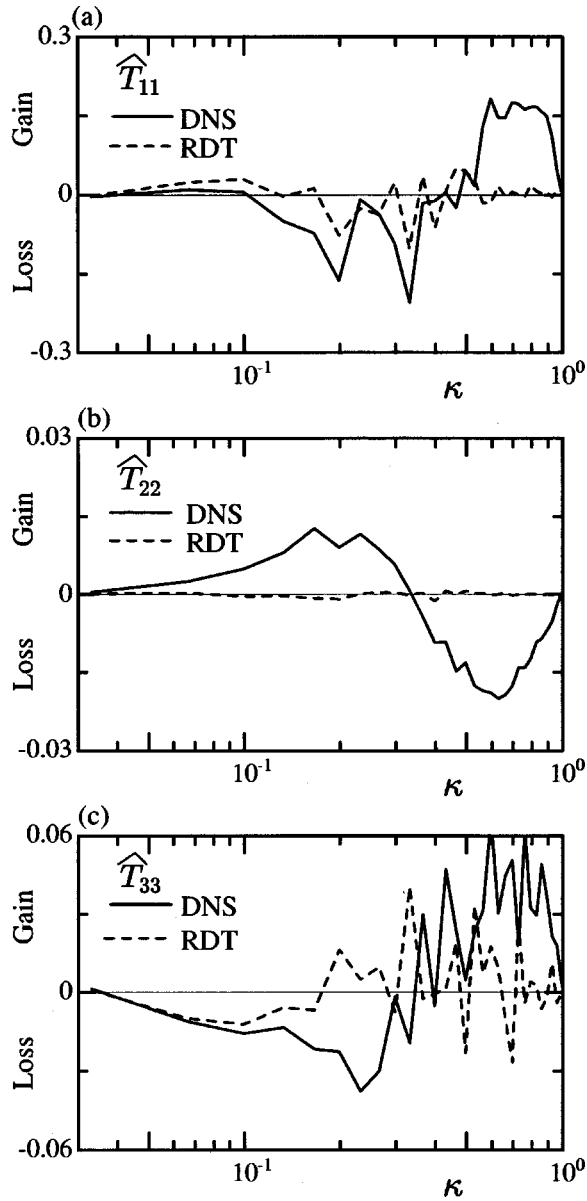


FIG. 14. Distributions of energy transfer functions in the spectral space. All wave numbers are nondimensionalized by S and ν . (a) \hat{T}_{11} , (b) \hat{T}_{22} , and (c) \hat{T}_{33} .

edly enhanced, in comparison to the case without it (RDT). Note that the transfer functions of RDT do not become zero because the isotropic turbulence used as the initial condition is not a Gaussian distribution. The differences between DNS and RDT are more marked in \hat{T}_{22} , which contributes to the inverse cascade of $\overline{u_2^2}$ in DNS as observed by Shirani *et al.*⁶

The transfer functions of the diagonal components $\hat{T}_{\alpha\alpha}$ can be divided into three terms; i.e., $\hat{T}_{\alpha\alpha,1}$, $\hat{T}_{\alpha\alpha,2}$, $\hat{T}_{\alpha\alpha,3}$ [see Eq. (11)]. The distributions of each component are shown in Fig. 15. It is noted that the second term, $\hat{T}_{11,2}$, contributes to the loss of turbulent kinetic energy in the low wave numbers, while the gain in the high wave numbers is associated with the third term $\hat{T}_{11,3}$. The combined effects of $\hat{T}_{11,2}$ and $\hat{T}_{11,3}$ are responsible for the energy cascade of $\overline{u_1^2}$.

Next, the association between the energy transfer func-

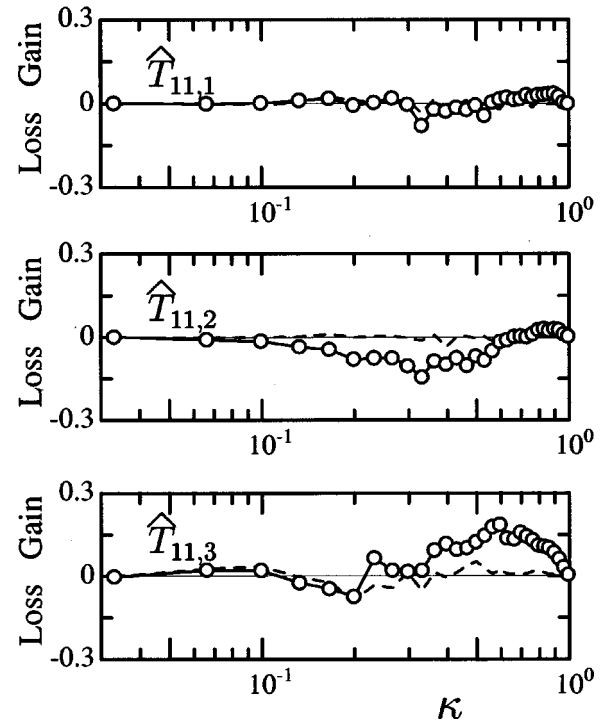


FIG. 15. Distributions of $\hat{T}_{11,j}$. Lines with symbols: DNS, dashed lines: RDT.

tions and the kinematics of the vortical structure is discussed. In the physical space, the transfer function $\hat{T}_{\alpha\alpha}$ can be written as

$$\begin{aligned}
 T_{\alpha\alpha} &= -u_k \frac{\partial u_\alpha^2}{\partial x_k} = -2u_\alpha \left(u_k \frac{\partial u_\alpha}{\partial x_k} \right) \\
 &= \underbrace{-2u_\alpha \left(u_1 \frac{\partial u_\alpha}{\partial x_1} \right)}_{T_{\alpha\alpha,1}} + \underbrace{-2u_\alpha \left(u_2 \frac{\partial u_\alpha}{\partial x_2} \right)}_{T_{\alpha\alpha,2}} + \underbrace{-2u_\alpha \left(u_3 \frac{\partial u_\alpha}{\partial x_3} \right)}_{T_{\alpha\alpha,3}}.
 \end{aligned} \tag{12}$$

Equation (12) gives the (inviscid) time derivative of the terms contributing to the velocity component variances (the diagonal elements of the Reynolds stress tensor). We form the distribution function of these terms with respect to the second invariant II . From these distributions, we determine the contribution of the vortices ($II > 0$) in the evolution of the Reynolds stresses.

Figure 16 shows the expected values of $T_{11,2}$ and $T_{11,3}$ versus the second invariant of the deformation tensor. It is noted that in the region $II > 0$, $T_{11,2}$ becomes negative, while $T_{11,3}$ takes a positive value there. Hence, the longitudinal vortices associated with $II > 0$ contribute to the energy cascade of $\overline{u_1^2}$ associated with $T_{11,2}$ and $T_{11,3}$. In the RDT results, the expected values of both $T_{11,2}$ and $T_{11,3}$ become almost zero.

In the following, the distribution of $-u_1 u_2$ and $\partial u_1 / \partial x_2$ included in $T_{11,2}$ will be discussed. As was shown in Fig. 9, $\partial u_1 / \partial x_2$ becomes negative in the region $II > 0$ because the

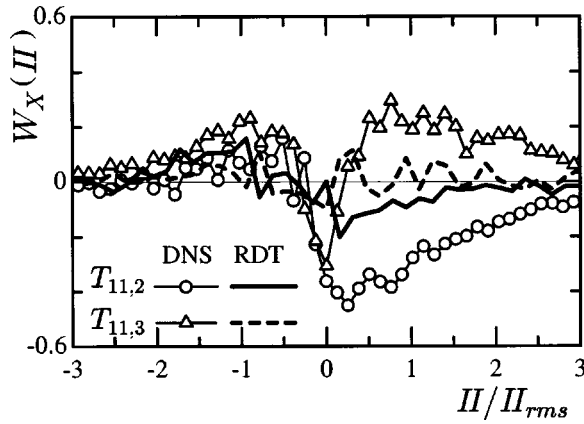


FIG. 16. Distributions of the expected values of the transfer functions versus II . Here $T_{11,2} = -2u_1u_2 \partial u_1 / \partial x_2$, $T_{11,3} = -2u_1u_3 \partial u_1 / \partial x_3$.

longitudinal vortices are wrapped by the streamwise velocity fluctuation u_1 , while it becomes zero in RDT without any convective motion. The instantaneous Reynolds shear stress $-u_1u_2 > 0$ is generated inside the streamwise vortices with the imposed mean shear $\partial U_1 / \partial x_2$ [see Fig. 17(a)]. Hence, the wrapping of the streamwise velocity fluctuation around the longitudinal vortices makes $T_{11,2} (= -2u_1u_2 \partial u_1 / \partial x_2)$ negative, which contributes to the loss of the energy u_1^2 and enhances the energy cascade. On the other hand, as discussed in Jeong *et al.*, $-u_1u_3$ is predominantly positive for the clockwise vortex ($\partial u_1 / \partial x_3 > 0$), while it becomes negative for the anticlockwise vortex ($\partial u_1 / \partial x_3 < 0$) because of the wrapping of u_1 , as shown in Fig. 17(b). Hence, $-2u_1u_3 \partial u_1 / \partial x_3$ becomes positive and contributes to the gain of the energy u_1^2 .

Next, we discuss the energy transfer functions \hat{T}_{22} and \hat{T}_{33} . As shown in Fig. 14, \hat{T}_{22} contributes to the inverse energy cascade, while the energy cascade associated with \hat{T}_{33} is enhanced by the nonlinear term. By illustrating the three parts [see Eq. (11)] included in the energy transfer functions \hat{T}_{22} and \hat{T}_{33} in Fig. 18, it is found that $\hat{T}_{22,3}$ is responsible for the inverse energy cascade of u_2^2 , while $\hat{T}_{33,2}$ enhances the energy cascade of u_3^2 .

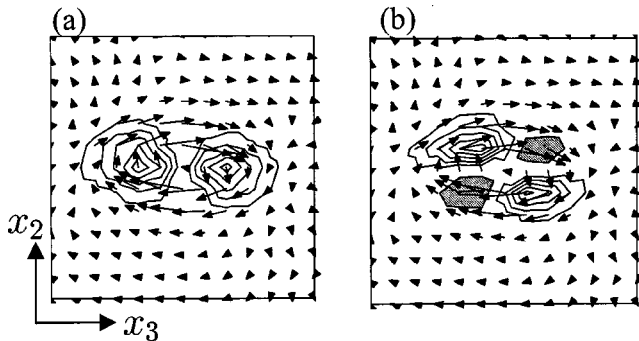


FIG. 17. Velocity vectors and contours of $-u_1u_2$ and $-u_1u_3$ in the x_2 - x_3 plane. The contour lines are plotted (a) for $-u_1u_2$ from 0.5 to 2.5 with an increment of 0.5, and (b) for $-u_1u_3$ from -2.0 to 5.0 with an increment of 1.0. The shaded regions represent the negative value. Both figures are results of DNS.

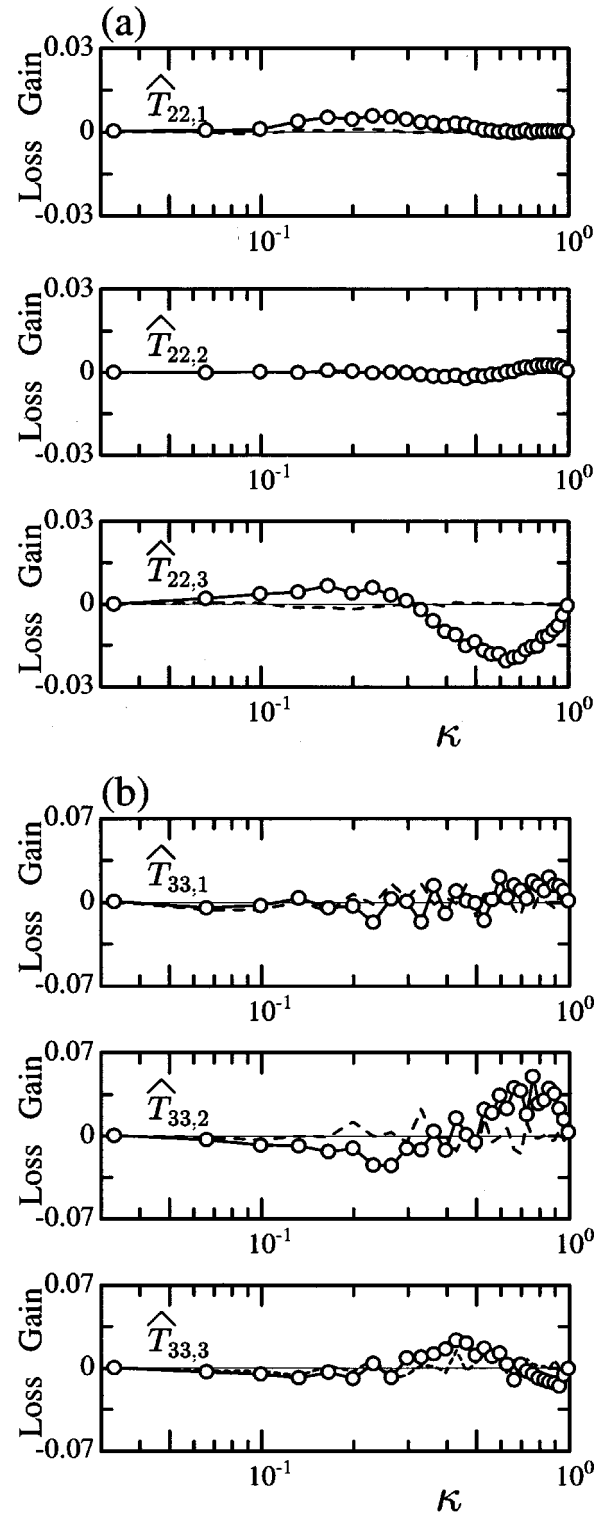
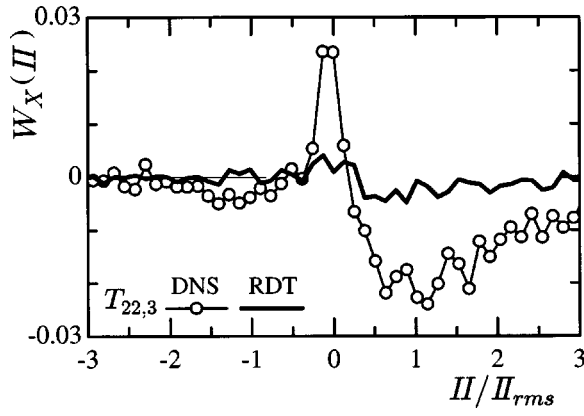


FIG. 18. Distributions of (a) $\hat{T}_{22,j}$ and (b) $\hat{T}_{33,j}$. Lines with symbols: DNS, dashed lines: RDT.

Figure 19 shows the expected values of $T_{22,3}$ vs II . The term $T_{22,3}$, which in the spectral space contributes to the loss of energy at the high wave numbers, becomes negative mainly in the region $II > 0$, indicating that the longitudinal vortices contribute to the loss of the energy u_2^2 .

Moreover, $T_{22,3}$ can be divided into two components that

FIG. 19. The expected value of $T_{22,3} = -2u_2u_3 \partial u_2 / \partial x_3$ vs Π .

are associated with the rotation and strain-rate tensor, respectively,

$$-u_3 \frac{\partial u_2^2}{\partial x_3} = -2u_3u_2 \frac{\partial u_2}{\partial x_3} = u_2u_3\omega_1 - 2u_2u_3s_{23}. \quad (13)$$

Figure 20 shows the distribution of each term on the rhs of Eq. (13). The rotational component $u_2u_3\omega_1$ is found to be responsible for the negative value of $T_{22,3}$ in the region $\Pi > 0$. This is as expected because the clockwise streamwise vortex ($\omega_1 > 0$, $\partial u_2 / \partial x_3 < 0$) contributes to the generation of $-u_2u_3 > 0$, while inside the anticlockwise vortex ($\omega_1 < 0$, $\partial u_2 / \partial x_3 > 0$), $-u_2u_3 < 0$ is generated.

When the energy transfer function $T_{33,2}$ is divided into the rotational and strain-rate components, the following equation is obtained:

$$-u_2 \frac{\partial u_3^2}{\partial x_2} = -2u_3u_2 \frac{\partial u_3}{\partial x_2} = -u_2u_3\omega_1 - 2u_2u_3s_{23}. \quad (14)$$

The rotational component $u_2u_3\omega_1$ contributes to the transfer function $T_{33,2}$ in the opposite direction from $T_{22,3}$. As a result, $T_{33,2}$ takes a positive value inside the streamwise vortex, enhancing the energy cascade of $\overline{u_3^2}$. Figure 21 shows the schematics for how the kinematics of the streamwise vortices affects the energy transfer functions. The generation of the streamwise velocity fluctuations and their wrapping around the streamwise vortices are correlated with the energy cas-

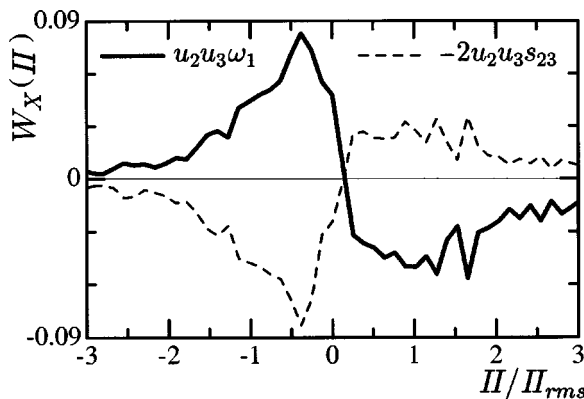
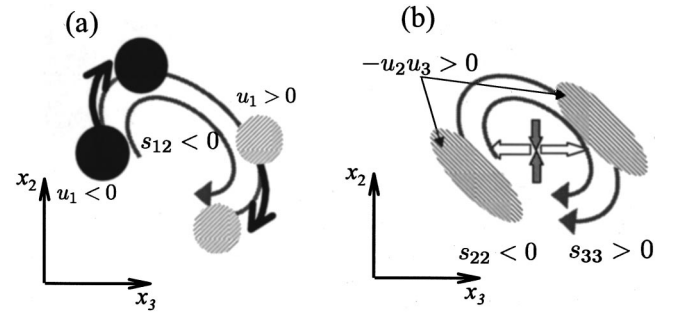
FIG. 20. The expected value of $u_2u_3\omega_1$ and $-2u_2u_3s_{23}$ vs Π .

FIG. 21. The schematics illustrating the association between the kinematics of the vortical structure and the energy transfer functions. (a) The generation of the streamwise velocity fluctuations and their wrapping around the streamwise vortices are correlated with the energy cascade of $\overline{u_1^2}$; (b) the strain-rates $\partial u_2 / \partial x_2 < 0$, $\partial u_3 / \partial x_3 > 0$ inside the vortices are associated with the energy transfer function T_{22} and T_{33} .

cade of $\overline{u_1^2}$. On the other hand, the strain rates $\partial u_2 / \partial x_2 > 0$, $\partial u_3 / \partial x_3 < 0$ inside the vortices are associated with the energy transfer function T_{22} and T_{33} .

III. CONCLUSIONS

Direct numerical simulations of a homogeneous shear flow are conducted to investigate the kinematics of the longitudinal vortices that are elucidated and conditionally averaged to obtain the most probable vortical structure. The results of DNS are compared with the RDT prediction to elucidate the effects of nonlinear terms. The association between the kinematics of the vortical structure and the energy transfer functions is also discussed in detail. As a result, the following conclusions are obtained.

(1) In a homogeneous shear flow, longitudinal vortices are generated, which inclined and tilted in the $x-y$ and $x-z$ planes, respectively. A similar inclination and tilting of the longitudinal vortices is observed in a turbulent channel flow.¹⁸ RDT can predict the inclination of the longitudinal vortex, while the tilting does not occur without an effect of the nonlinear terms.

(2) With the nonlinear term, the kinematics of the longitudinal vortex is affected by the strain-rate tensor; compression is in the vertical direction ($s_{22} < 0$), and the stretching is in both the streamwise and spanwise directions. These strain rates are associated with the spiral streamline in the streamwise direction and with the generation of the Reynolds shear stress $-u_2u_3$. The streamwise fluctuations generated at the sides of the streamwise vortex are wrapped around the vortex, in the course of which the strain rate, s_{12} , becomes negative.

(3) As a result of the strain rate imposed, the distribution of the slow pressure-strain correlation develops in the longitudinal vortices as follows:

$$\begin{aligned} 2(p_s/\rho)\partial u_1/\partial x_1 < 0, \quad 2(p_s/\rho)\partial u_2/\partial x_2 > 0, \\ 2(p_s/\rho)\partial u_3/\partial x_3 < 0. \end{aligned} \quad (15)$$

It is also found that inside the vortices, the distribution of the pressure-strain correlation is again closely similar between the homogeneous shear and turbulent channel flows.

(4) The energy transfer function of $\overline{u_1^2}$ contributes to the energy cascade, which is closely associated with the wrapping of the streamwise velocity fluctuations via the longitudinal vortices.

(5) The energy transfer function of $\overline{u_2^2}$ contributes to the inverse energy cascade, i.e., the mechanism whereby the energy in the spectral space is reconverted from high wave numbers to low wave numbers. On the other hand, the energy cascade of $\overline{u_3^2}$ is enhanced by its transfer function. It is also found that the transfer functions of $\overline{u_2^2}$ and $\overline{u_3^2}$ are both affected by generation of the Reynolds shear stress, $-u_2u_3$, associated with the longitudinal streamwise vortices.

ACKNOWLEDGMENTS

This work was supported by the Ministry of Education, Science, Sports, and Culture through a Grant-in-Aid for Scientific Research (B) (No. 10450085). The first and second authors are grateful to A. Ohyama for his assistance. All authors also wish to thank the referees for their helpful comments and suggestions.

¹S. J. Kline, W. C. Reynolds, F. A. Schraub, and P. W. Runstadler, "The structure of turbulent boundary layers," *J. Fluid Mech.* **30**, 741 (1967).

²S. K. Robinson, "The kinematics of turbulent boundary layer structure," NASA TM-103859, 1991.

³O. Iida and Y. Nagano, "The relaminarization mechanisms of turbulent channel flow at low Reynolds numbers," *Flow, Turbulence Combustion* **60**, 193 (1998).

⁴M. J. Lee, J. Kim, and P. Moin, "Structure of turbulence at high shear rate," *J. Fluid Mech.* **216**, 561 (1990).

⁵K. Lam and S. Banerjee, "On the condition of streak formation in a bounded turbulent flow," *Phys. Fluids A* **4**, 306 (1992).

⁶E. Shirani, J. H. Ferziger, and W. C. Reynolds, "Mixing of a passive scalar in isotropic and sheared homogeneous turbulence," Department of Mechanical Engineering, Report No. TF-15, Stanford University, 1981.

⁷M. M. Rogers, P. Moin, and W. C. Reynolds, "The structure and modeling of the hydrodynamic and passive scalar fields in homogeneous turbulent shear flow," Department of Mechanical Engineering, Report No. TF-25, Stanford University, 1986.

⁸S. Kida and M. Tanaka, "Reynolds stress and vortical structure in a uniformly sheared turbulence," *J. Phys. Soc. Jpn.*, **61**, 4400 (1992).

⁹S. Kida and M. Tanaka, "Dynamics of vortical structures in a homogeneous shear flow," *J. Fluid Mech.* **274**, 43 (1994).

¹⁰A. Matsumoto, Y. Nagano, and T. Tsuji, "Effects of mean shear on homogeneous turbulence," *Trans. JSME* **60B**, 1653 (1994).

¹¹A. M. Savil, "Recent developments in rapid-distortion theory," *Annu. Rev. Fluid Mech.* **19**, 531 (1987).

¹²J. C. R. Hunt and D. J. Carruthers, "Rapid distortion theory and the 'problems' of turbulence," *J. Fluid Mech.* **212**, 497 (1990).

¹³T. S. Lundgren, "Strained spiral vortex model for turbulent fine structure," *Phys. Fluids* **25**, 2193 (1982).

¹⁴R. S. Rogallo, "Numerical experiments in homogeneous turbulence," NASA TM-81315, 1981.

¹⁵J. C. R. Hunt, A. A. Wray, and P. Moin, "Eddies, streams, and convergence zones in turbulent flows," in *Proceedings of the 1988 Summer Program* (Stanford University, Stanford, CA, 1988), pp. 193–208.

¹⁶M. S. Chong, A. E. Perry, and B. J. Cantwell, "A general classification of three-dimensional flow fields," *Phys. Fluids A* **2**, 765 (1990).

¹⁷N. Kasagi, Y. Sumitani, Y. Suzuki, and O. Iida, "Kinematics of the quasi-coherent vortical structure in near-wall turbulence," *Int. J. Heat Fluid Flow* **16**, 2 (1995).

¹⁸J. Jeong, F. Hussain, W. Schoppa, and J. Kim, "Coherent structures near the wall in a turbulent channel flow," *J. Fluid Mech.* **332**, 185 (1997).

¹⁹W. T. Ashurst, A. R. Kerstein, R. M. Kerr, and C. H. Gibson, "Alignment of vorticity and scalar gradient with strain rate in simulated Navier–Stokes turbulence," *Phys. Fluids* **30**, 2343 (1987).

²⁰J. Jimenez and P. Moin, "The minimal flow unit in near-wall turbulence," *J. Fluid Mech.* **225**, 213 (1991).

²¹Y. Guezennec, D. Stretch, and J. Kim, "The structure of turbulent channel flow with passive scalar transport," in *Proceedings of the 1990 Summer Program* (Stanford University, Stanford, CA, 1990), pp. 127–138.